





# Lipid-based and protein-based interactions synergize transmembrane signaling stimulated by antigen clustering of IgE receptors

Nirmalya Bag<sup>a,1</sup> , Alice Wagenknecht-Wiesner<sup>a</sup>, Allan Lee<sup>a</sup>, Sophia M. Shi<sup>a</sup>, David A. Holowka<sup>a</sup>, and Barbara A. Baird<sup>a,1</sup> 

<sup>a</sup>Department of Chemistry and Chemical Biology, Cornell University, Ithaca, NY 14853

Edited by Jennifer Lippincott-Schwartz, Janelia Farm Research Campus, Ashburn, VA, and approved July 6, 2021 (received for review December 28, 2020)

**Antigen (Ag) crosslinking of immunoglobulin E-receptor (IgE-FcεRI) complexes in mast cells stimulates transmembrane (TM) signaling, requiring phosphorylation of the clustered FcεRI by lipid-anchored Lyn tyrosine kinase. Previous studies showed that this stimulated coupling between Lyn and FcεRI occurs in liquid ordered (Lo)-like nanodomains of the plasma membrane and that Lyn binds directly to cytosolic segments of FcεRI that it initially phosphorylates for amplified activity. Net phosphorylation above a nonfunctional threshold is achieved in the stimulated state but not in the resting state, and current evidence supports the hypothesis that this relies on Ag crosslinking to disrupt a balance between Lyn and tyrosine phosphatase activities. However, the structural interactions that underlie the stimulation process remain poorly defined. This study evaluates the relative contributions and functional importance of different types of interactions leading to suprathreshold phosphorylation of Ag-crosslinked IgE-FcεRI in live rat basophilic leukemia mast cells. Our high-precision diffusion measurements by imaging fluorescence correlation spectroscopy on multiple structural variants of Lyn and other lipid-anchored probes confirm subtle, stimulated stabilization of the Lo-like nanodomains in the membrane inner leaflet and concomitant sharpening of segregation from liquid disordered (Ld)-like regions. With other structural variants, we determine that lipid-based interactions are essential for access by Lyn, leading to phosphorylation of and protein-based binding to clustered FcεRI. By contrast, TM tyrosine phosphatase, PTPα, is excluded from these regions due to its Ld-preference and steric exclusion of TM segments. Overall, we establish a synergy of lipid-based, protein-based, and steric interactions underlying functional TM signaling in mast cells.**

transmembrane signaling | plasma membrane domains | rafts | Imaging FCS | FcεRI

Transmembrane (TM) signaling stimulated by antigen (Ag) occurs through cell surface immunoreceptors that lack a cytosolic kinase module, thus requiring tyrosine phosphorylation mediated by intermolecular coupling with a separate, plasma membrane-localized kinase (1). Effective coupling corresponds to a suprathreshold level of receptor phosphorylation that surmounts dephosphorylation by proximal tyrosine phosphatases. Orchestrated modulation of interactions among the signaling proteins (i.e., receptor, kinase, and phosphatase) (2, 3) and with other proteins [e.g., actin cytoskeleton (4)] are key to Ag-stimulated TM signaling. Although signaling studies have tended to focus on protein-protein interactions, contributions by collective lipid-based interactions are increasingly appreciated. In particular, phase-like organization of the plasma membrane provides capacity for colocalizing receptor and kinase while segregating phosphatase, according to their phase preferences (5). However, the relative importance remains a subject of debate (6–11), largely because it is experimentally difficult to separate the signaling contributions of lipid-based interactions from those of protein-based interactions in live cells.

Our group has worked to develop biophysical approaches that systematically delineate signaling interactions in the context of a

prototypical immunoreceptor signaling system: the high-affinity receptor for immunoglobulin E (IgE), FcεRI, in rat basophilic leukemia (RBL) mast cells (12, 13). Crosslinking of IgE-FcεRI by soluble, multivalent Ag creates FcεRI nanoclusters (14, 15) that are phosphorylated by Lyn, a src-family tyrosine kinase anchored to the inner leaflet of the plasma membrane by saturated acyl chains (Fig. 1A). Phosphorylated tyrosines on cytosolic β- and γ-subunits of FcεRI provide direct binding sites for Lyn's SH2 module to amplify the phosphorylation activity and create a binding site for Syk kinase and consequent assembly of a protein-based signaling platform that incorporates LAT scaffold and links to activation of phospholipase C-γ and attachment to the actin cytoskeleton (16). In mast cells, stimulated coupling of clustered FcεRI with Lyn initiates the cascade of cellular signaling and responses that underlie allergy and inflammation (12).

The role of lipids in stimulated Lyn/FcεRI coupling has been scrutinized in experimental (15, 17–19) and theoretical (20) studies over two decades, yielding the view that Ag crosslinking stabilizes liquid ordered (Lo)-like nanodomains around the clustered IgE-FcεRI. Referred to commonly (and roughly) as “rafts,” these proteolipid organizational features of plasma membranes have variable properties that depend on cellular circumstance but generally resemble Lo domains that coexist with liquid disordered (Ld) regions

## Significance

Lipid organization of the plasma membrane is known to be important for facilitating protein interactions in transmembrane signaling. However, the orchestration of these interactions in live cells remains elusive. We employed imaging fluorescence correlation spectroscopy (ImFCS) to systemically investigate the interplay of lipids and proteins during mast cell signaling, initiated as phosphorylation of antigen-crosslinked immunoglobulin E-receptor (IgE-FcεRI) complexes by lipid-anchored Lyn kinase. We found that stabilized liquid ordered-like nanodomains around clustered FcεRI—which can be accessed by Lyn kinase but not by transmembrane phosphatase—provide essential spatial filtering that augments Lyn's binding and phosphorylating FcεRI while suppressing dephosphorylation by phosphatase. ImFCS provides quantitative evidence of the functional link between lipid-based membrane organization and transmembrane signaling in live cells.

Author contributions: N.B., D.A.H., and B.A.B. designed research; N.B., A.W.-W., A.L., and S.M.S. performed research; N.B., A.L., and B.A.B. analyzed data; and N.B. and B.A.B. wrote the paper.

The authors declare no competing interest.

This article is a PNAS Direct Submission.

Published under the PNAS license.

<sup>1</sup>To whom correspondence may be addressed. Email: bab13@cornell.edu and nb559@cornell.edu.

This article contains supporting information online at <https://www.pnas.org/lookup/suppl/doi:10.1073/pnas.2026583118/-DCSupplemental>.

Published August 25, 2021.

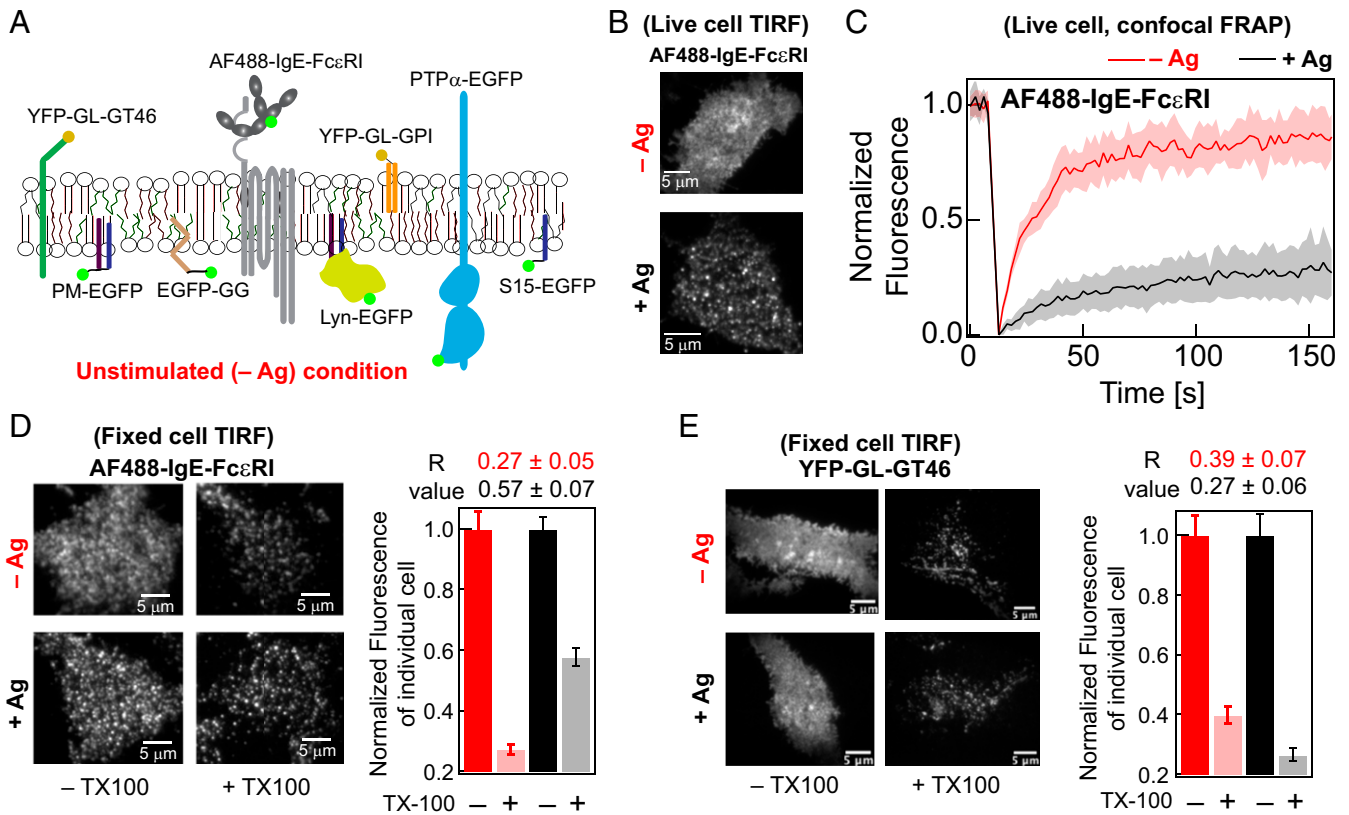


**Fig. 1.** AF488-IgE-Fc $\epsilon$ RI is clustered, partially immobilized, and exhibits elevated detergent resistance after crosslinking by soluble Ag (DNP-BSA) in RBL cells. (A) Plasma membrane localization in resting cells (-Ag) of AF488-IgE-Fc $\epsilon$ RI and other probes evaluated in this study. (B) Representative TIRF images of AF488-IgE-Fc $\epsilon$ RI on the ventral plasma membrane in live cells before (-Ag) and after (+Ag) stimulation by Ag. (C) Normalized FRAP curves of AF488-IgE-Fc $\epsilon$ RI obtained from individual cells are overlaid in -Ag (pink) and +Ag (gray) conditions. The solid red and black curves are average of the pink and gray curves, respectively. *SI Appendix, Fig. S1A* shows representative fitted FRAP data and box plots of recovery time and mobile fraction of all cells evaluated. (D) Representative fixed-cell TIRF images of AF488-IgE-Fc $\epsilon$ RI without (-TX100) and with (+0.04% TX100) treatment of both -Ag and +Ag conditions. Fluorescence retained after +TX100 treatment is normalized against corresponding -TX100 sample. The  $R$  values, corresponding to level of detergent resistance, are calculated from the ratio of median fluorescence of multiple cells in +TX100 to -TX100 samples (*SI Appendix, Eq. S2*). The error of  $R$  values was determined by bootstrapping as described in *SI Appendix*. (E) Representative fixed cell TIRF images under -/+Ag and -/+TX100 conditions and  $R$  values for YFP-GL-GT46. For each condition, 60 to 90 cells were imaged from at least two independent sample preparations for both AF488-IgE-Fc $\epsilon$ RI and YFP-GL-GT46. Box plots of fluorescence values for individual cells under -/+Ag and -/+TX100 conditions for both probes in representative experiments are provided in *SI Appendix, Fig. S2*.

at equilibrium in model membranes of defined composition (21). Experiments in cells show that Lyn kinase preferentially partitions into Lo-like nanodomains in the inner leaflet of the plasma membrane as mediated by its saturated lipid (palmitoyl/myristoyl, PM) anchor (15, 22, 23). By contrast, a TM tyrosine phosphatase, PTP $\alpha$ , and an inner-leaflet Ld-preferring lipid probe (geranylgeranyl, GG) preferentially localize to Ld-like regions, away from the Ag-clustered Fc $\epsilon$ RI (15, 23, 24). In early studies, the functional relevance of this lipid-driven spatial partitioning of the signaling components was shown by appearance of phosphorylated IgE-Fc $\epsilon$ RI in the Lo-like, detergent-resistant membrane (DRM) fraction only after Ag stimulation (24–26). Further functional evidence came from showing abrogated Fc $\epsilon$ RI phosphorylation after pharmacological depletion of cholesterol, a key component of Lo-like nanodomain formation (26). However, both DRM isolation and cholesterol depletion have known limitations (27), and they do not directly show whether lipid-based partitioning of Lyn is necessary or sufficient for functional coupling with clustered Fc $\epsilon$ RI.

In addition to the lipid-based partitioning into regions of clustered Fc $\epsilon$ RI, Lyn interacts directly with Fc $\epsilon$ RI- $\beta$  subunit by its cytosolic protein modules (SH3, SH2, and kinase modules). We showed previously that full-length Lyn is recruited to  $\mu$ m-scale Ag-patterned features more readily than its minimal PM lipid

anchor (17), indicating that protein binding stabilizes this interaction. Soluble Ag creates IgE-Fc $\epsilon$ RI nanoclusters, and their colocalization with Lyn (somewhat less with a PM lipid probe and not with a GG lipid probe) is observed using superresolution fluorescence microscopy and cross-correlation analysis (15). The relative low level of cross-correlation observed for Lyn and IgE-Fc $\epsilon$ RI clusters points to both lipid- and protein-based interactions being weak and dynamic. In general, the difference in phase-like organization of the plasma membrane between resting and stimulated states appears to be subtle and difficult to detect by conventional fluorescence microscopy and spectroscopy (15, 28, 29). Single-particle tracking (SPT) can be successful in picking up small changes. For example, Kusumi and colleagues developed high-speed SPT analysis built around a microscope dedicated to delineating transient interactions at single-molecule level (30, 31). Both superresolution and SPT approaches are technically demanding and typically require special fluorescent tags. As a complementary approach, we recently demonstrated that imaging fluorescence correlation spectroscopy (ImFCS) quantifies subtle differences in the diffusion properties of structurally distinct probes and subtle changes in the diffusion of a particular probe under different cell treatments (32). ImFCS images conventional fluorophores with a diffraction-limited total internal reflection fluorescence (TIRF) microscope (32,

33). These measurements yield probe diffusion coefficients ( $D$ ) in hundreds of pixel units simultaneously, and these measurements can be further extended over multiple cells to thousands of data points. Such large data statistics permit precise evaluation of  $D$ , thereby enabling detection of small changes in diffusion of a given probe that arises from the change in membrane organization. For example, by comparing Lo- and Ld-preferring probes, we previously detected changes in plasma membrane phase-like organization after inhibition of actin polymerization (32).

Faced with the challenge of delineating contributions of protein- and lipid-based interaction and subtle changes that occur in the plasma membrane after Ag-crosslinking of IgE-Fc $\epsilon$ RI, we have now improved the robustness of ImFCS data analysis, such that small changes are unambiguously determined. We evaluate ImFCS results, together with those from fluorescence recovery after photobleaching (FRAP) and a modified, image-based DRM assay (34), to compare biophysical properties of multiple probes (e.g., Fig. 1A), which, as a composite, represent membrane organization under resting (–Ag) and stimulated (+Ag) steady states of RBL cells. By evaluating diffusion properties of passive, inner-leaflet lipid probes with variable Lo-preference, we first characterize a relatively stable Lo-like environment around Ag-crosslinked Fc $\epsilon$ RI nanoclusters in the stimulated steady state. We construct Lyn variants to modify Lyn's lipid-based partitioning interactions, cytosolic protein-based interactions, and kinase activity. Comparative evaluation of variants reveals individual contribution of different interaction modes toward Lyn's coupling with Ag-clustered Fc $\epsilon$ RI. We show that the lipid-based partitioning of Lyn in the Lo-like nanodomains proximal to the Ag-clustered Fc $\epsilon$ RI increases the probability of the cytosolic protein-based interaction, thereby synergizing an efficient kinase/receptor coupling. We confirm that Lyn's Lo-preference is essential for stimulated phosphorylation of IgE-Fc $\epsilon$ RI in a reconstituted system. In contrast, our results provide evidence that TM tyrosine phosphatase, PTP $\alpha$ , is excluded from the region of Ag-clustered Fc $\epsilon$ RI because of the inherent Ld preference of PTP $\alpha$  and by steric hindrance of its TM segments. Overall, this study provides key experimental evidence to explain how cells utilize subtle changes in the phase-like lipid organization to enable protein–protein interactions necessary for initiating stimulated TM signaling.

## Results

Ag-crosslinking of IgE-Fc $\epsilon$ RI in RBL mast cells stimulates new interactions within the plasma membrane to facilitate suprathreshold Fc $\epsilon$ RI phosphorylation by Lyn tyrosine kinase as the first step of TM signaling. To delineate comprehensively the functional redistributions of lipids and proteins, we build on previous studies and use complementary approaches to monitor Ag-stimulated changes in diffusion and other properties over a range of selected probes (Fig. 1A and following figures). We find that shifts in distribution curves of diffusion coefficients derived from ImFCS provide an exceptionally sensitive representation of membrane changes that occur to initiate signaling.

**ImFCS Readily Detects Subtle Changes in Membrane Heterogeneity Caused by Ag Clustering of IgE-Fc $\epsilon$ RI.** Crosslinking of AlexaFluor488-labeled IgE-Fc $\epsilon$ RI (AF488-IgE-Fc $\epsilon$ RI; Fig. 1A) by Ag (DNP-BSA) in RBL plasma membranes forms distributed nanoclusters within 15 min that are visible by diffraction-limited TIRF microscopy (Fig. 1B). Our previous superresolution imaging showed that these individual nanoclusters have an average radius of  $\sim$ 80 nm (14). As previously measured by FRAP (35, 36) and confirmed here, 70% of the crosslinked AF488-IgE-Fc $\epsilon$ RI are immobile, and the 30% mobile fraction diffuse slower (i.e., longer fluorescence recovery time) than monomeric AF488-IgE-Fc $\epsilon$ RI present in resting cells (85% mobile; Fig. 1C and *SI Appendix, Fig. S1A*). By comparison, the yellow fluorescent protein (YFP)-tagged, Ld-preferring TM probe, YFP-GL-GT46 (comprising the TM segment of the low-

density lipoprotein receptor and the cytoplasmic tail of CD46) (37–39), has a mobile fraction of 84% with an insignificant shift in that value or the fluorescence recovery time after Ag crosslinking of IgE-Fc $\epsilon$ RI (*SI Appendix, Fig. S1B*).

Changes in resistance to detergent solubilization provided early evidence that crosslinked IgE-Fc $\epsilon$ RI nanoclusters associate with and stabilize Lo-like nanodomains (5, 15, 22, 24), as similarly documented for B and T cell receptors (34, 40–43). DRMs are Lo-like in lipid composition (44, 45) and retain coassociating proteins after solubilizing cells with 0.04% Triton X 100 (TX100) and floating on sucrose gradients (25). We recently adapted this basic methodology for evaluation of single cells by fluorescence microscopy (46), and we quantify the detergent resistance of a particular probe in the plasma membrane by a characteristic retention ( $R$ ) value.  $R$  is taken as the ratio of median fluorescence per cell after treatment with 0.04% TX100 to that of untreated cells (*SI Appendix, Eq. S2*). A larger  $R$  value reflects stronger interaction of the probe with membrane constituents that are not released under these conditions. We find that the  $R$  value of AF488-IgE-Fc $\epsilon$ RI increases from 0.3 to 0.6 after Ag crosslinking (Fig. 1D and *SI Appendix, S2A*). By comparison, the Ld-preferring TM probe YFP-GL-GT46 shows a slightly smaller  $R$  value after crosslinking IgE-Fc $\epsilon$ RI (0.4 to 0.3; Fig. 1E and *SI Appendix, S2B*). These distinctive behaviors are consistent with crosslinked AF488-IgE-Fc $\epsilon$ RI stabilizing Lo-like regions.

We recently established that diffusion properties of mobile membrane probes and their subtle changes after pharmacological treatments can be quantified precisely by TIRF-based ImFCS (32). This approach uses a fast camera and autocorrelates fluorescence fluctuations to determine diffusion coefficients ( $D$ ) of a particular probe at several hundreds of diffraction-limited spatial locations (Px unit = 320 nm  $\times$  320 nm) in single cells (Fig. 2A and B). The  $D$  value determined for an individual Px unit represents all nanoscopic environments that the probe moves through within that Px unit during the data acquisition time (280 s). Nanoscopic environments with more interactions (e.g., higher effective viscosity) yield a slower  $D$  value, and less-interactive environments yield a faster  $D$  value (Fig. 2B and C). By reflecting the interactions that structurally distinct probes experience, distinctive diffusion properties provide information about membrane organization. Pooling data from multiple cells yields  $\sim$ 10,000  $D$  values for a given probe, and the resulting high level of precision enables subtle differences in diffusion properties among probes to be discerned [(32); *SI Appendix, Table S1*]. As one measure of precision, the arithmetic average of pooled  $D$  values,  $D_{\text{av}}$ , has an SEM of less than 1% for every probe evaluated by ImFCS in this study (*SI Appendix, Table S1*).

The probability distribution functions (PDFs) of  $D$  values determined by ImFCS for mobile AF488-IgE-Fc $\epsilon$ RI from resting cells (red) and from cells stimulated with Ag (black) show a clear shift to slower  $D$  values after Ag is added (Fig. 2D), consistent with FRAP measurements (Fig. 1C and *SI Appendix, S1A*). To quantify possible subpopulations, we convert the pooled  $D$  values into cumulative distribution functions (CDFs; Fig. 2E)—a mathematically equivalent but bin-independent alternative to PDFs—which can be precisely resolved into one or two Gaussian components, parameterized as  $D_{\text{fast}}$ ,  $D_{\text{slow}}$ , and  $F_{\text{slow}}$  [*SI Appendix, Eqs. S3 and S4* (32)]. If a probe diffuses distinctively in subpopulations of Px units, the  $D$  CDF for this probe cannot be fitted by single Gaussian component ( $D_{\text{fast}} = D_{\text{slow}}$ ). Roughly interpreted,  $D_{\text{fast}}$  and  $D_{\text{slow}}$  represent the average diffusion coefficient of a particular probe in, respectively, interaction-poor and -rich subpopulations of Px units in the plasma membrane (Fig. 2C), and  $F_{\text{slow}}$  is the fraction of the interaction-rich population of Px units. To test whether CDF curves are overly influenced by outliers and to provide a curve thickness (related to level of uncertainty), we routinely resample the  $D$  values by bootstrapping 30 times (with 50% of all data each time), and the corresponding bootstrapped

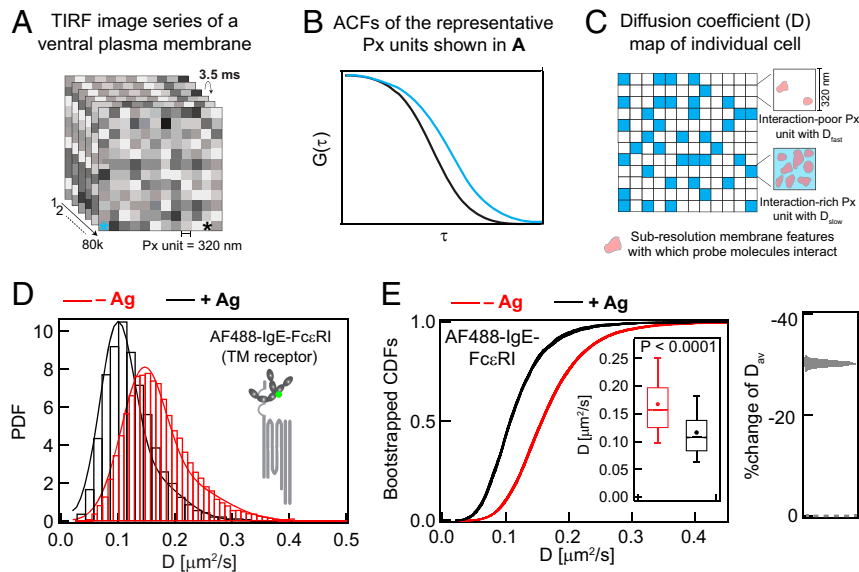


**Fig. 2.** Large datasets of ImFCS precisely characterize spatially heterogeneous diffusion of plasma membrane probes in both unstimulated ( $-Ag$ ) and stimulated ( $+Ag$ ) cells. (A and B) In a typical ImFCS recording, 80,000 TIRF microscopy images of fluorescently labeled ventral plasma membrane are collected at 3.5 ms/frame. The autocorrelation function (ACF) from a given Px unit ( $320\text{ nm} \times 320\text{ nm}$ ) decays faster if probes diffuse faster within that Px unit. The ACFs, corresponding to the Px units designated with asterisks of same color, illustrate probes diffusing slower (cyan) and faster (black). (C) Schematic diffusion coefficient ( $D$ ) map, obtained after ACF analyses of all Px units contains some Px units with relatively slower ( $D_{slow}$ , cyan) or faster ( $D_{fast}$ , white) diffusion coefficient, interpreted as interaction-rich and interaction-poor units, respectively. (D) Histograms of experimental  $D$  values ( $>10,000$ ; *SI Appendix, Table S1*) and PDF for AF488-IgE-FcεRI at  $-Ag$  (red) and  $+Ag$  (black) steady states. PDFs are fitted using parameters derived from bin-independent CDFs (*SI Appendix, Eq. A2*). (E) CDFs of the same  $D$  values as in part (D). Pooled  $D$  values are resampled 30 times by bootstrapping with 50% of all data each time, and individual bootstrapped CDFs are fitted for  $D_{slow}$ ,  $D_{fast}$ , and  $F_{slow}$  (*SI Appendix, Table S1*). Individual raw bootstrapped CDFs of  $D$  values of AF488-IgE-FcεRI at each condition are overlaid and shown (red:  $-Ag$  and black:  $+Ag$ ). (Inset) Box plots of all  $D$  values. Box height corresponds to 25th to 75th percentile; error bars represent 9th to 91st percentile of entire dataset; mean and median values are represented as solid circle and bar, respectively; notches signify 95% CI of the median. Right shows the stimulated  $\%change$  of  $D_{av}$ : Effect change distribution is calculated from the bootstrapped mean values at each condition.

CDFs are fitted individually (*SI Appendix*). For all probes tested in this study, we found narrowly distributed values of fitting parameters  $D_{fast}$ ,  $D_{slow}$ , and  $F_{slow}$ , confirming the reliability and robustness of our analysis (*SI Appendix, Table S1*). The  $D_{av}$  determined from ImFCS measurements of  $D$  across all Px units and the profile of the  $D$  CDFs reveal how structurally distinct probes sense changes in local environments caused by Ag-mediated clustering of IgE-FcεRI to stimulate TM signaling. Visually striking are the distinctive shifts in the bootstrapped CDF curves of  $D$  values that

accompany Ag stimulation (Figs. 2–6). Comparing these shifts in CDF curves and their representative  $D_{av}$  values for a panel of probes with defined structural features allows us to evaluate contributions of individual structural features to stimulated changes in diffusion properties. In this manner, we can infer how Ag-stimulation changes lipid- or protein-based interactions in the plasma membrane and corresponding changes in membrane organization.

After Ag-crosslinking AF488-IgE-FcεRI to form nanoclusters (14, 47), ImFCS measurements show the mobile fraction (30% as

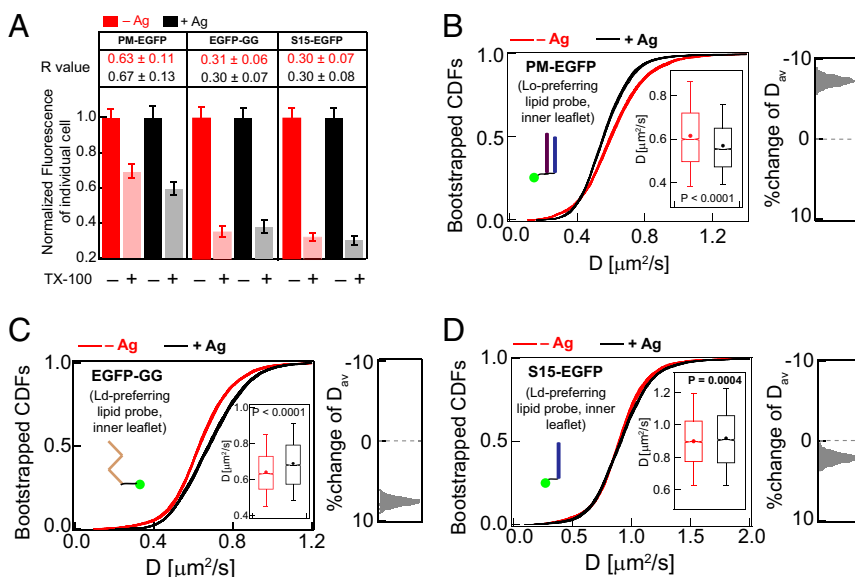


**Fig. 3.** ImFCS but not DRM detects subtle stabilization of Lo-like regions in Ag-stimulated RBL cells. (A) Degree of detergent resistance for PM-EGFP, EGFP-GG, and S15-EGFP and  $R$  values for  $-Ag$  (red) and  $+Ag$  (black) conditions. Box plots of fluorescence values of individual cells for  $-/+TX100$  and  $-/+Ag$  conditions for these probes are provided in *SI Appendix, Fig. S3*. (B–D) A total of 30 bootstrapped CDFs of  $D$  values from ImFCS measurements are overlaid for specified probes and conditions ( $-/+Ag$ ). Box plots of all  $D$  values and distribution of stimulated  $\%change$  of  $D_{av}$  as described for Fig. 2E. *SI Appendix, Table S1* shows number of autocorrelation function and cells measured for ImFCS analyses.

measured by FRAP; Fig. 1C and *SI Appendix, S1A*) has  $\sim 35\%$  smaller  $D_{av}$  ( $0.117 \pm 0.0005 \mu\text{m}^2/\text{s}$ ) than monomeric AF488-IgE-Fc $\epsilon$ RI in resting cells ( $0.168 \pm 0.0004 \mu\text{m}^2/\text{s}$ ) (*SI Appendix, Table S1*). Correspondingly, the PDFs and bootstrapped CDFs clearly shift to lower  $D$  values after stimulation with Ag (Fig. 2D and E). The effect size distribution of  $D_{av}$  further quantifies the amount and direction of diffusion change based on the bootstrapped CDF curves (Fig. 2E, Right). Mobile IgE-Fc $\epsilon$ RI in the stimulated steady state are likely to include small oligomers, which have been shown to be signaling competent (48). We find that Ag crosslinking of IgE-Fc $\epsilon$ RI imparts biophysical changes across and on both sides of the membrane. Stimulated modulation in diffusion of structurally distinct probes reflects these changes.

Evaluating Ag-stimulated changes in the lipid phase-like properties of the plasma membrane requires consideration of compositional differences in the outer- and inner-membrane leaflets. As recently characterized in erythrocyte plasma membranes, outer-leaflet lipids are more Lo-like, whereas inner-leaflet lipids are more Ld-like (49). Similarly, the outer leaflet of resting RBL cells was found to be more ordered when compared to the inner leaflet. We might then expect that Ag-stimulated changes in phase-like properties may manifest differently for the inner and outer leaflets. Because stimulated coupling of Lyn kinase with Ag-clustered Fc $\epsilon$ RI occurs in the inner leaflet of the plasma membrane, we first focused on stimulated changes in the Lo/Ld-like properties in this leaflet. For this purpose, we evaluated properties of inner-leaflet lipid probes that are phase selective but otherwise passive in the signaling process. We employed three genetically encoded probes that distinctively anchor enhanced green fluorescent protein (EGFP) to the inner leaflet [Fig. 1A (23, 50)]: PM-EGFP, with palmitoyl and myristoyl acyl chains [Lo-preferring (23)], EGFP-GG, with a GG chain and a polybasic protein sequence [Ld preferring (23)] and S15-EGFP, with a myristoyl chain and a polybasic protein sequence [Ld preferring (51)]. Our previous superresolution imaging demonstrated that the PM construct colocalizes with crosslinked IgE-Fc $\epsilon$ RI, but the GG construct does not (15), and consistent results were obtained with clustered B cell receptors (41). Diffraction-limited TIRF imaging reveals no visible changes in the distribution of any of these probes after Ag addition (*SI Appendix, Fig. S5*), and we examined their membrane interactions using DRM imaging, FRAP, and ImFCS.

For phase-selective lipid probes, a larger  $R$  value in the DRM assay indicates stronger partitioning into Lo-like nanodomains.

In resting cells, we found  $R$  values to be consistent with their phase preferences in membranes as reported previously (50–52): PM-EGFP ( $R = 0.6$ ) > EGFP-GG (0.3) = S15-EGFP (0.3) (Fig. 3A and *SI Appendix, Fig. S3*, red/pink). Although these  $R$  values are useful for monitoring Lo- versus Ld-phase preference of these lipid probes, we found the method to be insufficiently sensitive for detecting significant differences before and after Ag-crosslinking of IgE-Fc $\epsilon$ RI (Fig. 3A and *SI Appendix, Fig. S3*, compare red/pink to black/gray). Similarly, FRAP measurements do not resolve significant differences for any of these probes before and after stimulation (*SI Appendix, Fig. S4*). In contrast, Ag-crosslinking of IgE-Fc $\epsilon$ RI causes distinctive shifts in the ImFCS CDF curves for each of these probes (Fig. 3B–D): Lo-preferring probe PM-EGFP shifts to slower  $D$  values, and Ld-preferring probes EGFP-GG and S15-EGFP shift to faster  $D$  values. In terms of  $D_{av}$  values (*SI Appendix, Table S1*), the shifts are 8% slower for PM-EGFP ( $0.62 \pm 0.002$  to  $0.57 \pm 0.002 \mu\text{m}^2/\text{s}$ ), 8% faster for EGFP-GG ( $0.64 \pm 0.002$  to  $0.69 \pm 0.002 \mu\text{m}^2/\text{s}$ ), and 2% faster for S15-EGFP ( $0.90 \pm 0.003$  to  $0.92 \pm 0.003 \mu\text{m}^2/\text{s}$ ). These contrasting behaviors of Lo- and Ld-preferring lipid probes are consistent with the Lo-like phase in the inner leaflet of the plasma membrane becoming more ordered and stabilized against surrounding Ld-like regions, which become more disordered after Ag addition. These ImFCS measurements on inner-leaflet lipid probes before and after stimulation are consistent with and extend quantitative results from previous superresolution imaging (15). Collectively, they characterize and quantify stabilization of a Lo-like environment encompassing Ag-crosslinked IgE-Fc $\epsilon$ RI nanoclusters in the membrane inner leaflet.

**Lo-Preference of Lipid Anchor Is Necessary for Lyn's Functional Coupling with Crosslinked IgE-Fc $\epsilon$ RI.** Nanoscopic colocalization of Lyn with crosslinked IgE-Fc $\epsilon$ RI nanoclusters was observed by superresolution cross-correlation imaging as a threefold enhancement in Lyn density in these regions compared with other parts of the membrane (15). This low level of stimulated modulation in Lyn interactions is not detectable in TIRF images, DRM  $R$  values, or FRAP curves (*SI Appendix, Fig. S6 A–C*). However, ImFCS sensitively detects the subtle change by resolving a shift of the CDF curves to lower  $D$  values (Fig. 4A), corresponding to 10% reduction of  $D_{av}$  of Lyn-EGFP after Ag addition (from  $0.49 \pm 0.001$  to  $0.44 \pm 0.001 \mu\text{m}^2/\text{s}$ ; *SI Appendix, Table S1*). Lyn-EGFP is highly detergent resistant [ $R = 0.8$ ; Fig. 5A (28)], as expected for the Lo-preference of its PM

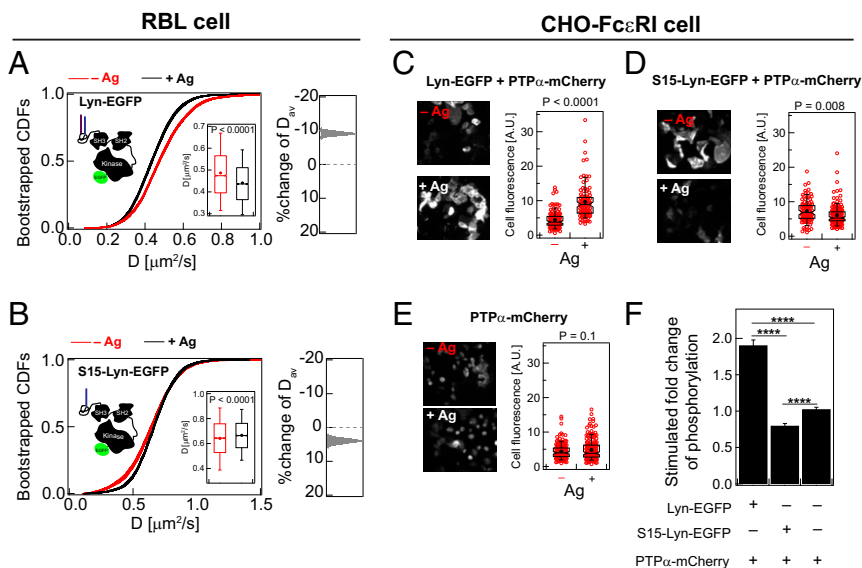


**Fig. 4.** Lipid-driven Lo-preference of Lyn is necessary for its functional coupling with Ag-crosslinked IgE-Fc $\epsilon$ RI. A total of 30 bootstrapped CDFs of  $D$  values from ImFCS measurements in RBL cells are overlaid for WT Lyn-EGFP (A) and the Ld-preferring Lyn chimera S15-Lyn-EGFP (B) in  $-/+$ Ag conditions. Box plots of all  $D$  values and stimulated  $\%$ change of  $D_{av}$  are shown as described for Fig. 2E. *SI Appendix, Table S1* shows number of autocorrelation function and cells measured for ImFCS analyses. (C–E) Representative images of immunostained phosphorylation for CHO cells stably transfected with Fc $\epsilon$ RI and transiently transfected with specified Lyn variant and PTP $\alpha$ . Red circles are fluorescence of individual cells for a representative biological replica, and the box plots are defined as described in Fig. 2E. (F) Quantification of stimulated changes of phosphorylation for each condition. \*\*\*\*:  $P < 10^{-4}$  (unpaired Student's  $t$  test).

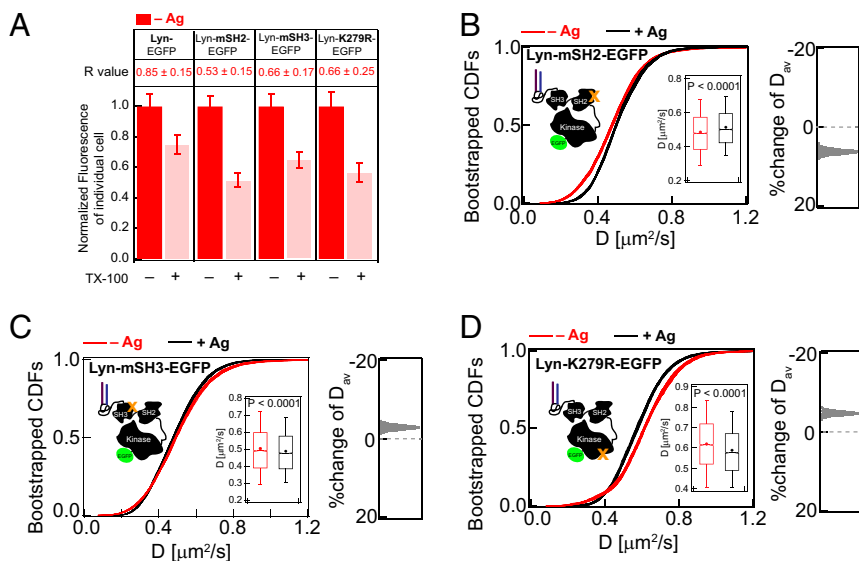


**Fig. 5.** Cytosolic protein modules of Lyn-EGFP contribute to detergent-resistance and reduction of diffusion caused by Ag-crosslinking of IgE-Fc $\epsilon$ RI. (A) Detergent resistance of Lyn-EGFP compared to variants Lyn-mSH2-EGFP, Lyn-mSH3-EGFP, and Lyn-K279R-EGFP as represented by relative loss of fluorescence after TX100 treatment and corresponding  $R$  values in unstimulated (-Ag) RBL cells. Box plots of fluorescence values of individual cells for -/+TX100 and -/+Ag conditions for these probes are provided in *SI Appendix, Figs. S6B* (Lyn-EGFP) and *S7A* (Lyn-EGFP variants). (B-D) 30 bootstrapped CDFs of  $D$  values from ImFCS measurements are overlaid for specified probes and conditions (-/+Ag). Box plots of all  $D$  values and stimulated %change of  $D_{av}$  are shown as described for Fig. 2E. *SI Appendix, Table S1* shows number of autocorrelation function and cells measured for ImFCS analyses.

membrane anchor and consistent with the stimulated shift in this probe's diffusion properties being the consequence of more stable Lo-like nanodomains after Ag crosslinking of IgE-Fc $\epsilon$ RI. However, the degree of shifts in the CDF curves are different for Lyn-EGFP (Fig. 4A) compared to PM-EGFP (Fig. 3B), as quantified by the effect size distributions of  $D_{av}$  for these two probes (Right panels in Figs. 3B and 4A). These differences indicate that some of Lyn-EGFP interactions in stimulated cells occur directly with the crosslinked Fc $\epsilon$ RI, in addition to those with the surrounding stabilized Lo-like regions into which the PM lipid anchor partitions favorably.

To deconvolve lipid- and protein-based interactions, we compared diffusion modes of Lyn-EGFP in both resting and stimulated states to a Lyn chimera. S15-Lyn-EGFP was created by replacing the first 15 amino acids of wild-type (WT) Lyn,

which possesses Lo-targeting palmitoylation and myristoylation sites, with the first 15 amino acids of Ld-preferring lipid probe S15-EGFP containing a single myristoyl site and a polybasic region (51). Unlike Lyn-EGFP, S15-Lyn-EGFP exhibits little detergent-resistance ( $R = 0.2$ ; *SI Appendix, Fig. S6B*) and has a faster  $D_{av}$  in resting cells ( $D_{av} = 0.64 \pm 0.002 \mu\text{m}^2/\text{s}$ ; Fig. 4B and *SI Appendix, Table S1*). S15-Lyn-EGFP serves as a Lyn probe that anchors to the inner leaflet by an Ld-preferring lipid but possesses Lyn's functional protein modules. If protein-protein interactions primarily drive stimulated reduction of Lyn-EGFP diffusion, we expect to see similar net change of diffusion of S15-Lyn-EGFP after Ag-crosslinking of IgE-Fc $\epsilon$ RI. However, in sharp contrast to Lyn-EGFP (Fig. 4A), the  $D_{av}$  value of S15-Lyn-EGFP (Fig. 4B) does not decrease after Ag addition but rather increases to  $0.67 \pm 0.002 \mu\text{m}^2/\text{s}$  (5% faster), similar to the

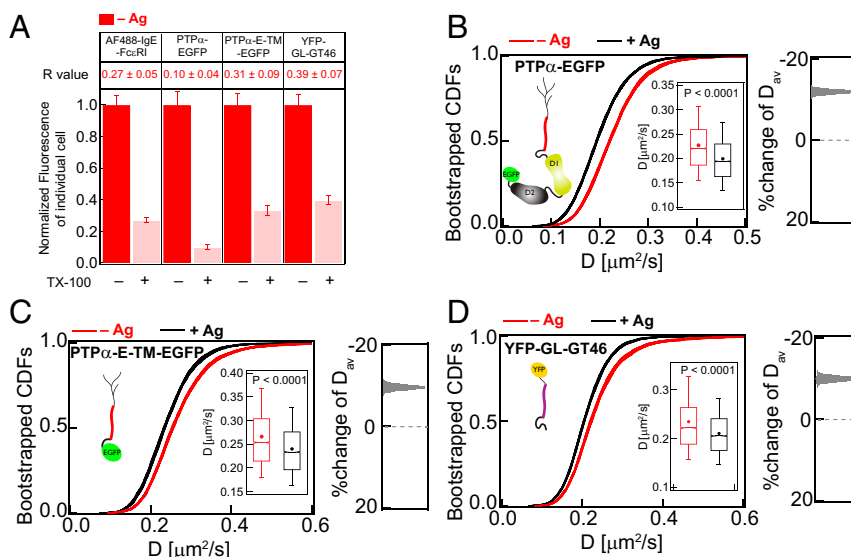


**Fig. 6.** TM probes are strongly detergent soluble but show relatively slower diffusion in stimulated cells. (A) Detergent resistance of AF488-IgE-Fc $\epsilon$ RI, PTP $\alpha$ -EGFP, PTP $\alpha$ -E-TM-EGFP, and YFP-GL-GT46 as represented by relative loss of fluorescence after TX100 treatment and corresponding  $R$  values in unstimulated (-Ag) RBL cells. Box plots of fluorescence values of individual cells for -/+TX100 and -/+Ag conditions for these probes are provided in *SI Appendix, Figs. S2* (AF488-IgE-Fc $\epsilon$ RI and YFP-GL-GT46) and *S8A* (PTP $\alpha$ -EGFP and PTP $\alpha$ -E-TM-EGFP). (B-D) A total of 30 bootstrapped CDFs of  $D$  values from ImFCS measurements are overlaid for specified probes and conditions (-/+Ag). Box plots of all  $D$  values and stimulated %change of  $D_{av}$  are shown as described for Fig. 2E. *SI Appendix, Table S1* shows number of autocorrelation function and cells measured for ImFCS analyses.

behavior of Ld-preferring lipid probes, EGFP-GG and S15-EGFP (Fig. 3 C and D and *SI Appendix, Table S1*). Although the trend appears similar, the data statistics of FRAP are not sufficient to resolve these differences between Lyn and S15-Lyn (*SI Appendix, Fig. S6 C and D*).

The slower diffusion of Lyn-EGFP and faster diffusion of S15-Lyn-EGFP after crosslinking IgE-Fc $\epsilon$ RI revealed by ImFCS represent a subtle but distinguishable change in the phase-like organization that is sensed by Lo- and Ld-preferring probes. These ImFCS results for Lyn-EGFP and S15-Lyn-EGFP are consistent with the view that Lo-preference is necessary for Lyn's interaction with clustered IgE-Fc $\epsilon$ RI. Changes in diffusion for Lyn-EGFP compared to PM-EGFP points to a role for protein-based interactions for optimal coupling leading to receptor phosphorylation and downstream signaling.

**Lyn-EGFP but not S15-Lyn-EGFP Facilitates Ag-Dependent Tyrosine Phosphorylation.** To test directly a functional outcome inferred from our ImFCS results, we compared the capacities of Lyn-EGFP and S15-Lyn-EGFP to facilitate stimulated phosphorylation in cells. We used a reconstitution approach for this purpose: Fc $\epsilon$ RI stably expressed in Chinese hamster ovary cells (CHO-Fc $\epsilon$ RI) that are transiently cotransfected with Lyn and an Ld-preferring TM tyrosine phosphatase  $\alpha$  (PTP $\alpha$ ). With this experimental system, we found previously that PTP $\alpha$  suppresses Lyn kinase activity and minimizes its spontaneous phosphorylation of Fc $\epsilon$ RI, while facilitating Ag-stimulated Fc $\epsilon$ RI phosphorylation (24). This previous study also showed that a PTP $\alpha$  chimera anchored to the inner leaflet by Lo-preferring lipids (PM) fails to reconstitute Ag-dependent Fc $\epsilon$ RI phosphorylation. In the current study, we used immunostaining to monitor tyrosine phosphorylation in CHO-Fc $\epsilon$ RI cells transiently transfected with mCherry tagged WT PTP $\alpha$  (PTP $\alpha$ -mCherry) and either Lyn-EGFP or S15-Lyn-EGFP before and after addition of Ag. As shown in Fig. 4 C–F, cotransfection with Lyn-EGFP causes a nearly twofold enhancement of tyrosine phosphorylation, compared to no Lyn construct, whereas cotransfection with S15-Lyn-EGFP results in a somewhat reduced level of tyrosine phosphorylation. Results from this functional assay are consistent with ImFCS diffusion measurements and show that Lo-preference is essential for Lyn's colocalization with clustered IgE-Fc $\epsilon$ RI but leaving open the possibility that protein-based interactions are also involved.

**Intact Protein Modules of Lyn Are Necessary for Its Effective Coupling with Crosslinked IgE-Fc $\epsilon$ RI.** The cytosolic segments of Lyn comprise an SH2 module that docks on phosphotyrosine (pY) sites, an SH3 module which interacts with polyproline (PxxP) motifs, and a kinase module (53). To test the importance of direct interactions with Fc $\epsilon$ RI in stimulated cells, we evaluated the diffusion properties of two point mutants (54): Lyn-mSH2-EGFP (Arg to Ala at position 135) and Lyn-mSH3-EGFP (Trp to Ala at position 78), with intact PM lipid anchor but disabled binding capabilities through SH2 and SH3 modules, respectively. In resting cells, the detergent resistance of both mutants ( $R = \sim 0.6$ ; *SI Appendix, Fig. S7A*) is less than Lyn-EGFP ( $R = 0.8$ ; Fig. 5A), similar to PM-EGFP ( $R = 0.6$ ; Fig. 3A) and greater than Ld-preferring S15-Lyn-EGFP ( $R = 0.2$ ; *SI Appendix, Fig. S6B*). Changes in diffusion properties of Lyn variants after Ag crosslinking of IgE-Fc $\epsilon$ RI are not resolved by FRAP (*SI Appendix, Fig. S7 B–D*) but revealed by ImFCS (Fig. 5 B and C). ImFCS further reveals clear differences for Lyn-mSH2-EGFP and Lyn-mSH3-EGFP compared to Lyn-EGFP in terms of stimulated shifts in CDF curves. After Ag addition, the  $D_{av}$  values for Lyn-EGFP decrease (Fig. 4A), increase slightly for Lyn-mSH2-EGFP (Fig. 5B), and decrease slightly for Lyn-mSH3-EGFP (Fig. 5C). Also, Lyn-mSH2-EGFP responds differently from PM-EGFP (Fig. 3B) to stimulated stabilization of Lo-like nanodomains, even though it is similarly detergent resistant. One possible

explanation for differences is cytosolic steric hindrance due to scaffold proteins and cytoskeleton components that are recruited to Ag-crosslinked IgE-Fc $\epsilon$ RI (13, 55, 56). Lo-preferring lipid, PM-EGFP, with no Lyn protein modules in the cytoplasm, is likely to be less sensitive to these steric factors. Unlike Lyn-EGFP, Lyn-mSH2-EGFP and Lyn-mSH3-EGFP cannot efficiently overcome steric hindrance by docking at the pY219 site on clustered Fc $\epsilon$ RI. It appears that Ag-induced changes in Lyn diffusion compared to these two Lyn mutants depend on interactions with Fc $\epsilon$ RI rather than entirely on their Lo-preference.

We measured the stimulated diffusion change of kinase-inactive Lyn mutant, Lyn-K279R-EGFP (57), to test whether phosphorylation of Fc $\epsilon$ RI by Lyn stabilizes the coupling of these two proteins. In resting cells, similar to Lyn-mSH2-EGFP and Lyn-mSH3-EGFP, Lyn-K279R-EGFP shows weaker detergent resistance ( $R = 0.6$ ) compared to WT Lyn-EGFP (Fig. 5A and *SI Appendix, S7A*). This consistent difference suggests that kinase activity and resulting protein-based interactions contribute to Lyn's greater tendency to localize in a Lo-like environment. Lyn-K279R-EGFP, unlike Lyn-mSH2-EGFP and Lyn-mSH3-EGFP, is expected to undergo proper SH2/pY219 intermolecular docking after Fc $\epsilon$ RI phosphorylation by the endogenous Lyn present in these cells (57). However, the shift in the CDF curve to lower diffusion coefficients is less for Lyn-K279R-EGFP (5% decrease of  $D_{av}$ :  $0.62 \pm 0.002$   $\mu\text{m}^2/\text{s}$ ; Fig. 5D) compared to Lyn-EGFP (10% decrease of  $D_{av}$ :  $0.49 \pm 0.001$  to  $0.44 \pm 0.001$   $\mu\text{m}^2/\text{s}$ ; Fig. 4A), suggesting competitive advantage of endogenous Lyn over Lyn-K279R in associating with phosphorylated Fc $\epsilon$ RI.

Collectively, the shifts in CDF curves (Figs. 4 A and B and 5 B–D) of Lyn-EGFP compared to the Lyn variants we tested support the following view: the Lo-preference of Lyn, as mediated by saturated lipid anchors, is essential for its coupling with Ag-crosslinked Fc $\epsilon$ RI; Lyn's kinase activity and Fc $\epsilon$ RI-docking capacities secondarily serve to stabilize the interaction.

**TM PTP $\alpha$  Exclusion from Ag-Crosslinked Fc $\epsilon$ RI Nanoclusters Is Accompanied by Its Slowed Diffusion.** Raising the phosphorylated state of Ag-crosslinked Fc $\epsilon$ RI above the stimulation threshold requires that access by phosphatases be minimized. Previous studies (5, 22, 24, 58) support the hypothesis that tyrosine phosphorylation of Fc $\epsilon$ RI by Lyn kinase prior to Ag engagement is counterbalanced by TM phosphatase-mediated dephosphorylation: Transient nanodomains present in the resting steady state do not sufficiently confine Lo-preferring Lyn and monomeric Fc $\epsilon$ RI nor prevent access by phosphatase to disrupt the balance. Nanodomains that are stabilized around the Ag-clustered Fc $\epsilon$ RI preferentially include kinase, exclude phosphatase, and tip the balance to exceed the phosphorylation threshold. We examined participation of the TM phosphatase within this mechanism by measuring stimulated changes in diffusional and other properties of EGFP-tagged PTP $\alpha$  variants.

Consistent with our previous observations that PTP $\alpha$  prefers an Ld-like environment (24), we found that PTP $\alpha$ -EGFP exhibits little detergent resistance in resting cells ( $R = 0.1$ ; Fig. 6A and *SI Appendix, S8A*). ImFCS measurements of this probe in resting cells yields  $D_{av} = 0.227 \pm 0.0006$   $\mu\text{m}^2/\text{s}$ . This value is similar to other single-pass TM probes reported previously (32, 59) and slower than inner- or outer-leaflet lipid probes (32, 38) or inner-leaflet lipid-anchored proteins such as Lyn kinase ( $0.49 \pm 0.001$   $\mu\text{m}^2/\text{s}$ ; *SI Appendix, Table S1*). This is not surprising because the diffusion of TM probes is influenced by their interactions within both membrane leaflets and with extracellular and cytosolic components. After Ag addition, PTP $\alpha$ -EGFP is expected to be excluded from regions of crosslinked IgE-Fc $\epsilon$ RI because of its Ld preference. Interestingly, however, we found that  $D_{av}$  for PTP $\alpha$ -EGFP decreases by 12% (to  $0.199 \pm 0.0005$   $\mu\text{m}^2/\text{s}$ ) after Ag addition (Fig. 6B and *SI Appendix, Table S1*). This direction in stimulated change of  $D_{av}$  is same as for inner-leaflet,

Lo-preferring lipid probes (PM-EGFP and Lyn-EGFP) and opposite to that of inner-leaflet, Ld-preferring probes (EGFP-GG, S15-EGFP, and S15-Lyn) (Fig. 7A). These comparisons raise intriguing questions and indicate minimally that the stimulated diffusion change of TM PTP $\alpha$ -EGFP is not controlled by modulation of lipid organization in the membrane inner leaflet.

To consider whether diffusion of TM probes is influenced by Ag-stimulated modulation of outer-leaflet phase-like properties, we evaluated YFP-tagged glycosylphosphatidylinositol (YFP-GL-GPI), a Lo-preferring lipid probe. Although neither DRM assays ( $R = \sim 1$ ) nor FRAP resolve differences between resting and Ag-stimulated cells for YFP-GL-GPI (SI Appendix, Fig. S9A and B), ImFCS revealed a stimulated decrease in  $D_{av}$  ( $0.328 \pm 0.0008 \mu\text{m}^2/\text{s}$  to  $0.276 \pm 0.0009 \mu\text{m}^2/\text{s}$ , 16%; SI Appendix, Fig. S9C and Table S1). This might be expected if Ag clustering of IgE-Fc $\epsilon$ RI stabilizes more ordered lipids around these clusters in the outer leaflet. However, the relative decrease in  $D_{av}$  for YFP-GL-GPI is similar to that of Ld-preferring PTP $\alpha$ -EGFP, which suggests another possibility: If the outer leaflet is primarily Lo-like in resting cells (49), stimulated reduction in diffusion observed for both probes may point to globally increased ordering in this leaflet that occurs with Ag crosslinking of IgE-Fc $\epsilon$ RI and stimulated signaling.

Another, nonexclusive explanation for slowed diffusion of PTP $\alpha$ -EGFP arises from considering other effects caused by Ag, which crosslink and immobilize IgE-Fc $\epsilon$ RI (Fig. 1B and C). Theoretical studies considering hydrodynamic and steric interactions between membrane components indicate that the presence of immobile objects, even at very low surface coverage (5%), decreases diffusion of other mobile objects (60–62). These predictions led us to test whether the diffusion of TM probes generally decrease after Ag stimulation creates new diffusion obstacles, minimally those in the form of immobilized TM domains within the Fc $\epsilon$ RI nanoclusters. To consider this possibility, we created a PTP $\alpha$  construct, PTP $\alpha$ -E-TM-EGFP, which includes the extracellular module and TM domain (TMD) of PTP $\alpha$  and is C terminally fused to EGFP (as illustrated in Fig. 6C). Because this probe does not contain the catalytic or other cytosolic modules of PTP $\alpha$ , any Ag-stimulated change of its diffusion is not due to functional interactions with Fc $\epsilon$ RI. PTP $\alpha$ -E-TM-EGFP in resting cells has low detergent resistance ( $R = 0.3$ , Fig. 6A) and FRAP similar to PTP $\alpha$ -EGFP (SI Appendix, Fig. S8B and C). ImFCS determined  $D_{av}$  ( $0.266 \pm 0.0008 \mu\text{m}^2/\text{s}$ ) for PTP $\alpha$ -E-TM-EGFP in resting cells is slightly greater than that for PTP $\alpha$ -EGFP (SI Appendix, Table S1), possibly due to eliminated cytosolic interactions. After Ag crosslinking of IgE-Fc $\epsilon$ RI,  $D_{av}$  for PTP $\alpha$ -E-TM-EGFP decreases by 11%, and the shift in ImFCS CDF curves is strikingly similar to the shift for PTP $\alpha$ -EGFP (Fig. 6B and C). These results indicate that Ag-stimulated reduction of PTP $\alpha$  diffusion is not due to functional interactions with other proteins. We observed a similar 13% stimulated decrease in  $D_{av}$  for YFP-GL-GT46, another Ld-preferring but passive TM probe (Fig. 6D). These experimental results are consistent with the possibility that immobilization of Fc $\epsilon$ RI after Ag-clustering creates new diffusion obstacles that slow diffusion of other TM proteins on the length scale measured by ImFCS. They also provide evidence that exclusion of PTP $\alpha$ -EGFP from Ag-clustered Fc $\epsilon$ RI is due in part to steric hindrance.

## Discussion

Nanoclustering of TM receptors by extracellular ligands followed by local reorganization in the plasma membrane to facilitate kinase coupling and receptor phosphorylation above a stimulation threshold has become a general paradigm of signaling through cell surface immunoreceptors. A large body of evidence supports the view that Ag-mediated nanoclustering of sensitized mast cell receptors, IgE-Fc $\epsilon$ RI, coalesces proteolipid nanodomains that have Lo-like character (5, 6, 63). However, the functional significance of lipid phase-like behavior in TM

signaling mediated by this and other immunoreceptors continues to be debated (21, 64, 65), and some have taken the position that stimulated protein–protein interactions are sufficient (3). Although protein-based interactions may increasingly dominate as signaling proceeds, the initial upshift in receptor phosphorylation appears to depend on disrupting the balance between kinase and phosphatase access, and this is mediated by membrane lipids. Simply stated, stabilization of Lo-like nanodomains around Ag-crosslinked immunoreceptors serves to colocalize Lo-preferring lipid-anchored kinase (e.g., Lyn), while Ld-preferring TM phosphatases (e.g., PTP $\alpha$ ) are excluded. In this study, we used ImFCS measurements that build on other imaging approaches to quantify systematically the subtle shift in plasma membrane organization that accompanies Ag-mediated stimulation. We confirm the primacy of lipid-based interactions and unveil how these synergize with protein-based interactions among IgE-Fc $\epsilon$ RI, Lyn kinase, and PTP $\alpha$  phosphatase. We evaluate particular contributions of these different types of interactions for functional assembly of TM signaling components.

We previously established ImFCS as a statistically robust approach for quantifying differences in the diffusion properties of selected probes that collectively sense the organization of the plasma membrane under specified conditions (32). The sampling provided by our ImFCS measurements ( $\sim 10,000$   $D$  values for each probe) yields extremely precise CDF curves and values for  $D_{av}$ . As we demonstrate herein, ImFCS measurements of 14 independent, structurally distinct probes sensitively reveal subtle changes in plasma membrane organization that result from Ag-stimulation. These changes are simply represented by  $D_{av}$  values and distinguished by the shifts in CDF curves of all  $D$  values (Figs. 2–6 and summarized in Fig. 7A). Ag-stimulated differences are quantified by effect size distributions of  $D_{av}$  and by detailed changes in the fit parameters of the CDF curves (SI Appendix, Table S1). By systematically evaluating key structural features among the selected probes and corresponding differences in their diffusion properties measured before and after Ag stimulation, we can minimally reconstruct participation of different types of interactions experienced by the initial signaling components as illustrated in Fig. 7B.

**Ag Crosslinking Creates Nanoclusters of IgE-Fc $\epsilon$ RI and Stabilizes Surrounding Lo-Like Domains in the Membrane Inner Leaflet.** Because the plasma membrane is asymmetric in lipid composition, we focused primarily on the inner leaflet, where membrane-anchored Lyn phosphorylates Fc $\epsilon$ RI after its clustering by Ag. In general, the phase-like behavior of the plasma membrane in resting cells can be approximated by the tendency of Lo-preferring probes to be more detergent resistant than Ld-preferring probes. Consistent with previous results, we found in resting cells that Lo-preferring PM-EGFP and Lyn-EGFP to be more detergent resistant than Ld-preferring EGFP-GG and S15-EGFP (Fig. 3A and SI Appendix, Fig. S6B). However, the Lo-like domains in this resting state appear to be small and transient (21), with relative weak distinction from Ld-like regions, as suggested by ImFCS measurement of small differences in  $D_{av}$  values for PM-EGFP and EGFP-GG [(32); SI Appendix, Table S1]. This relatively weak phase-like heterogeneity in the cell's resting state would allow access to monomeric Fc $\epsilon$ RI by both Lyn kinase and TM phosphatase and thereby limit net phosphorylation (66). That Ag crosslinking of IgE-Fc $\epsilon$ RI leads to proximal coalescence and stabilization of Lo-like domains in the inner leaflet was clearly indicated previously by reconstitution studies (24) and by superresolution imaging of coclustering with IgE-Fc $\epsilon$ RI by PM probes but not GG probes (15). However, this level of stabilization is not detected within the limited sensitivity of DRM imaging (Fig. 3) and FRAP measurements (SI Appendix, Fig. S4). In contrast, statistically robust ImFCS measurements show subtle but distinctive shifts in  $D$  CDF curves and  $D_{av}$  values for the Lo-preferring probes compared to Ld-preferring probes.



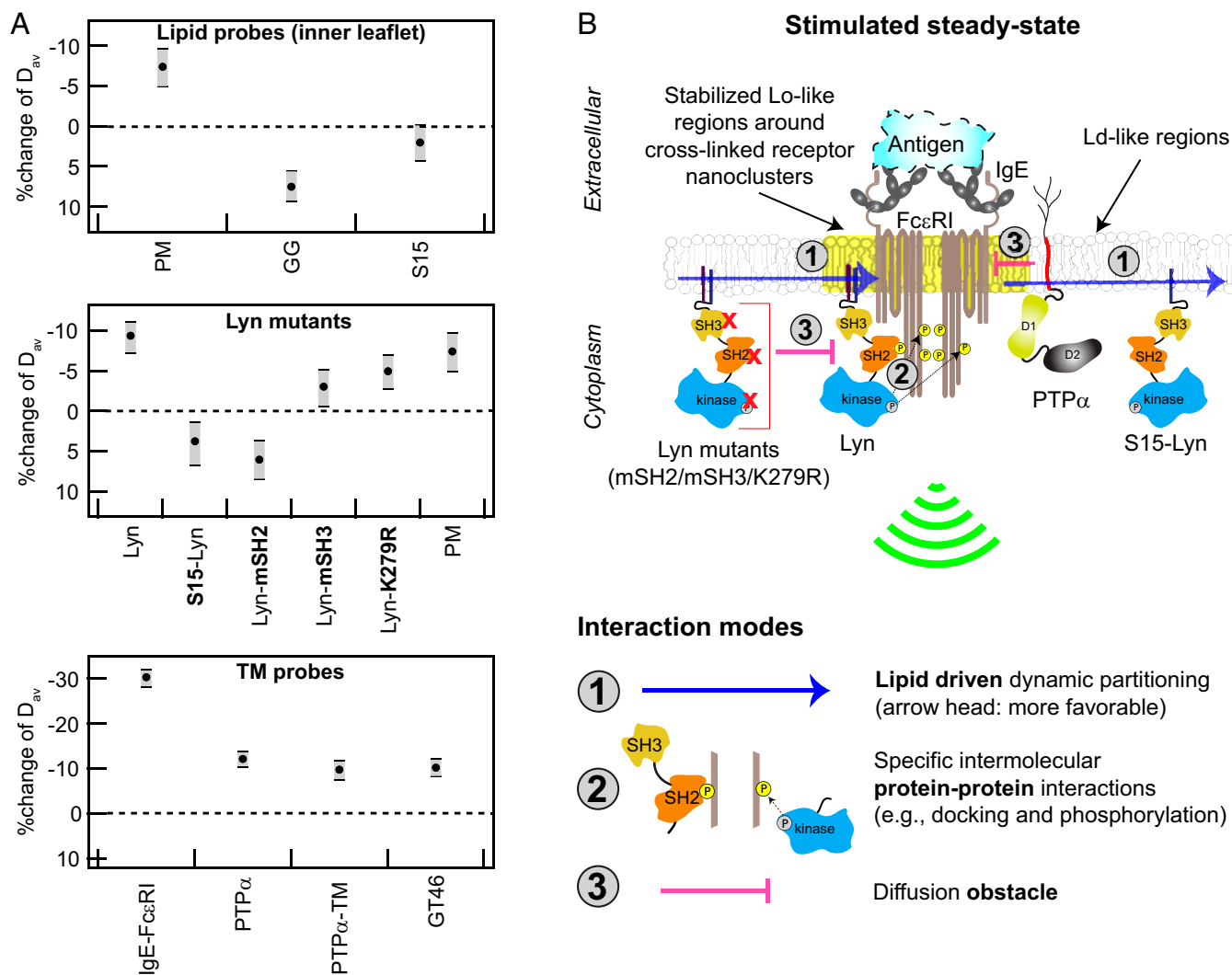


**Fig. 7.** Ag-crosslinking of IgE-FcεRI stabilizes surrounding Lo-like nanodomains, causing dynamic lipid- and protein-based interactions that shift diffusion properties of signaling components and lead to suprathreshold phosphorylation by Lyn. (A) Stimulated changes in  $D_{av}$  for inner leaflet lipid probes, Lyn variants, and TM probes, including IgE-FcεRI and PTPα. Values and error bars represent effect change distributions shown in Figs. 2–6. (B) Proposed interaction modes leading to functional coupling of Lyn with clustered FcεRI: Stabilized Lo-like environment preferentially includes Lo-preferring Lyn and excludes Ld-preferring S15-Lyn and PTPα (interaction mode 1). Preferentially proximal Lyn (interaction mode 1) phosphorylates clustered FcεRI via its kinase module and then binds to pTyr via its SH2 module as facilitated by its SH3 module (interaction mode 2); these cumulative interactions stabilize the coupling. Lyn variants with impaired kinase, SH2, or SH3 modules are sterically hindered by cytoplasmic segments of clustered FcεRI (interaction mode 3). PTPα, which is preferentially excluded from Lo-like environments (interaction mode 1), is further limited in access to FcεRI-pTyr due to steric hindrance by clustered FcεRI-TMDs (interaction mode 3).

The lipid-anchored probes are driven by their intrinsic partitioning preferences: PM-EGFP and Lyn-EGFP shift to slower diffusion in modulated Lo-like domains, whereas EGFP-GG and S15-EGFP shift to faster diffusion in proximal Ld-like regions (Figs. 3, 4, and 7A). Stabilization of a Lo-like environment that encompasses the clustered FcεRI on the membrane inner leaflet may represent a thermodynamic adjustment, such as overcoming a hydrophobic mismatch of the collected TMDs and surrounding lipids (67) or possibly biasing critical fluctuations (68). We and others used a two-dimensional (2D)-Ising model to show that, when exogenously clustered, membrane components with Lo-preference weakly coalesce with other Lo-preferring components (15, 20, 41, 43). This lipid rearrangement establishes a more distinctive, phase-like membrane organization in the Ag-stimulated steady state (15, 18, 19). Such remodeling of membrane organization on the inner leaflet would facilitate lipid-driven sorting of Lo- (e.g., Lyn) from Ld-preferring components as previously proposed (66).

The smaller decrease in diffusion for PM-EGFP compared to Lyn-EGFP is similar to the trend observed with superresolution imaging: the Lyn probe coclusters with Ag-crosslinked IgE-FcεRI somewhat more than PM (15). The differences indicate interactions of Lyn's cytosolic protein modules, in addition to its membrane anchor. To derive additional insight from shifts in the ImFCS CDF curves after Ag-stimulation, we can consider their precise fit parameters, which are based on a Gaussian model. This simple model is limited in providing physical information because quantified changes in diffusion (measured on the Px unit length scale) may involve multiple lipid-based factors (e.g., changes in lipid ordering, probe partitioning, and domain coverage), in addition to any protein-based interactions. All contributing factors are averaged together and represented as changes in populations of interaction-rich ( $D_{slow}$ ) or -poor ( $D_{fast}$ ) Px units [Fig. 2C (32)]. However, a reasonable interpretation can be made for inner-leaflet probes, which are localized primarily by the phase preference of

their lipid anchors. For example, a quantitative comparison of CDF curve shifts for Lyn-EGFP and PM-EGFP indicates that Lyn's cytosolic protein modules (SH2, SH3, and kinase) participate in its slowed diffusion. We find that both fit parameters  $D_{\text{fast}}$  and  $D_{\text{slow}}$  decrease for Lyn-EGFP, while only  $D_{\text{slow}}$  decreases for PM-EGFP after Ag stimulation (SI Appendix, Table S1). This comparison suggests that IgE-FcεRI clusters in the interaction-poor Px units do not adequately stabilize the Lo-like nanodomains to have an impact on the diffusion of PM-EGFP, which undergoes only lipid-based interactions. However, even relatively weak stabilization of Lo-like nanodomains in the interaction-poor Px units is sufficient to decrease the diffusion of Lyn-EGFP in these units due to its additional protein-based interactions with clustered IgE-FcεRI. We are currently exploring other fitting models to further exploit the quantitatively precise  $D$  CDF shapes and shifts, thereby to extract more detailed physical information about stimulated changes in membrane organization.

**Lyn Access to Ag-Crosslinked IgE-FcεRI on the Inner Leaflet Requires Lipid-Based Filtering and is Enhanced by Protein Binding.** Comparing Lyn-EGFP (Lo-preferring) to S15-Lyn-EGFP (Ld-preferring) confirms that lipid-based sorting into stabilized Lo-like domains is the primary requirement for Lyn's capacity to couple functionally with IgE-FcεRI. Unlike Lyn-EGFP and PM-EGFP,  $D_{\text{av}}$  values and CDF curves for S15-Lyn-EGFP shift to faster diffusion after Ag addition, similarly to EGFP-GG and S15-EGFP (Figs. 3, 4, and 7A). This comparison shows that interactions mediated by Lyn's cytosolic protein modules do not serve to slow diffusion unless Lyn's PM anchor steers it into stabilized Lo-like domains. We infer that the slowed diffusion of Lyn-EGFP corresponds to Lyn first partitioning into the Lo-like domains that surround Ag-crosslinked IgE-FcεRI [Fig. 7B, interaction mode 1 (15)]. Then, in this proximal location, Lyn phosphorylates tyrosines in cytosolic segments of FcεRI (pTyr) and transiently binds to these pTyr via its SH2 module [Fig. 7B, interaction mode 2 (69)]. In comparison, S15-Lyn does not appreciably undergo interaction mode 1, and PM lipid anchor does not undergo interaction mode 2 (Fig. 7B). These interaction differences, which produce contrasting diffusion shifts after Ag addition (Fig. 7A), also manifest functionally: Ag stimulates tyrosine phosphorylation mediated by Lyn-EGFP but not by S15-Lyn-EGFP (Fig. 4F).

ImFCS measurements on Lyn probes with variations in cytosolic protein modules further show that protein interactions participate in appropriate coupling with Ag-crosslinked IgE-FcεRI. We found that if SH2-mediated binding to phosphorylated FcεRI is prevented by a mutation in this module (54), then the diffusion of this Lyn-mSH2-EGFP variant shifts faster (rather than slower) after Ag addition (Figs. 5B and 7A). These results suggest that the clustered cytosolic segments of Ag-crosslinked FcεRI sterically hinder the cytosolic protein modules of this Lyn variant (Fig. 7B, interaction mode 3) to counteract lipid-based partitioning of its PM anchor. This interpretation is consistent with results for other Lyn variants. Unlike Lyn-mSH2-EGFP, the  $D$  CDFs and  $D_{\text{av}}$  values for Lyn-K279R-EGFP and Lyn-mSH3-EGFP shift to slightly slower diffusion after Ag-crosslinking of IgE-FcεRI, but the extent of this negative shift is less than that for Lyn-EGFP and PM-EGFP (Figs. 4, 5, and 7A). We expect kinase-inactive Lyn-K279R-EGFP to be steered to stabilized Lo-domains (via PM anchor; Fig. 7B, interaction mode 1) resulting in slower diffusion, and this variant has the capacity to bind to FcεRI tyrosines that are phosphorylated by endogenous Lyn in these cells (Fig. 7B, interaction mode 2). However, endogenous Lyn is likely to be more competitive for proximal binding to the tyrosines it phosphorylates, and accordingly, Lyn-K279R-EGFP is probably more sensitive to steric hindrance by the clustered cytosolic segments of FcεRI (Fig. 7B, interaction mode 3).

The Lyn-mSH3-EGFP variant has a PM anchor, kinase activity, and an intact SH2 module. However, the cytosolic SH3

module, which connects the PM anchor to SH2 and kinase modules, has been found to provide conformational plasticity of Lyn cytosolic segments for optimal catalytic activity and subsequent binding to pTyr in FcεRI (70). The impaired SH3 domain in Lyn-mSH3-EGFP is expected to limit this optimizing effect, rendering this variant more susceptible to steric hindrance by the clustered FcεRI. These ImFCS results are consistent with our previous observations that Lyn-mSH2-EGFP is not recruited, and Lyn-mSH3-EGFP is only weakly recruited to μm-scale IgE-FcεRI clusters that form when cells are placed on Ag-micropatterned surfaces (54). In contrast, both Lyn-EGFP and PM-EGFP are recruited to these micropatterned features (17, 54). Overall, the balance among interaction modes 1, 2, and 3 (Fig. 7B) after Ag addition results in slower diffusion for Lyn-K279R-EGFP and Lyn-mSH3-EGFP but distinctively smaller shifts than for Lyn-EGFP (Fig. 7A and B). We conclude that after Ag crosslinking of IgE-FcεRI, the primary coupling interaction is Lo-preference of Lyn's PM anchor to facilitate its phosphorylation of FcεRI cytosolic segments followed by binding of its SH2 module to stabilize further the interaction. Despite these stabilizing effects, the interactions are dynamic and relatively weak, such that the overall slowing of Lyn-EGFP diffusion is subtle (10% reduction in  $D_{\text{av}}$ ; Fig. 7A). The small magnitude of this change is consistent with the degree of coclustering of Lyn and Ag-crosslinked IgE-FcεRI observed with superresolution imaging (15).

**Slowed Diffusion of PTPα that Accompanies Exclusion from Ag-Clustered IgE-FcεRI Reflects Increased Ordering of the Outer Leaflet and Steric Hindrance.** Modulation of PTPα-EGFP's biophysical properties after Ag addition is consistent with exclusion from Ag-clustered FcεRI and points to involvement of multiple factors. That PTPα-EGFP has very low detergent resistance (Fig. 6A) agrees with our previous reconstitution studies (24) showing that this TM phosphatase prefers an Ld-like environment, thereby limiting its access to the stabilized Lo-like environment surrounding Lyn-phosphorylated FcεRI after Ag addition (Fig. 7B, interaction mode 1). More recently, we observed that PTPα is preferentially excluded from subclusters of IgE-FcεRI when cells are placed on Ag-patterned surfaces (71). For both studies, the effects were reversed when the extracellular and TM modules of PTPα were replaced by a Lo-preferring PM membrane anchor. Consistent with our results, superresolution imaging and cross-correlation analysis showed that Ld-preferring TM phosphatase CD45 is depleted from the vicinity of Ag-crosslinked B cell receptor clusters (43).

It is interesting that the  $D$  CDF curves (Fig. 6B) and  $D_{\text{av}}$  (Fig. 7A) for PTPα-EGFP shift to slower diffusion after Ag addition. This trend differs from stimulated changes in the diffusion of Ld-preferring lipid probes in the inner leaflet, showing that the diffusion of TM PTPα-EGFP is not controlled by the phase-like properties of the membrane inner leaflet. The membrane outer leaflet in resting RBL cells was found to be more ordered than the inner leaflet (49), and this differential lipid organization is consistent with our previously published result that outer-leaflet Lo-preferring probe YFP-GL-GPI diffuses much slower than the inner-leaflet Lo-preferring probe PM-EGFP in unstimulated cells (32). Our ImFCS measurements allow the possibility that Ag crosslinking of IgE-FcεRI increases the overall ordering in the outer leaflet through a mechanism that may involve the cytoskeleton but has not yet been established. For example, predominant Lo-like domains may become more ordered and connected, whereas Ld-like domains become more disordered and isolated. However, Ag-stimulated slowing of YFP-GL-GPI (SI Appendix, Fig. S9C) could also be explained by stabilization of more highly ordered nanodomains around Ag-clustered FcεRI in the outer leaflet, as suggested in our early imaging of DiIC<sub>16</sub> colocalizing with patches of highly crosslinked

IgE-FcεRI (72). Recently, high-speed single-particle tracking revealed transient arrest in the lateral diffusion of outer-leaflet, Lo-preferring sphingomyelin around Ag-clustered FcεRI, whereas outer leaflet, Ld-preferring dioleoylphosphatidylcholine shows no arrest (30). Our ImFCS measurements leave open the possibility that FcεRI clustering increases the ordering of outer-leaflet lipids overall, thereby slowing both Ld- and Lo-preferring probes that experience this leaflet.

Exclusion of an Ld-preferring TM phosphatase from Ag-clustered FcεRI probably involves stabilizing a more ordered environment proximally and steric hindrance by FcεRI TM segments (Fig. 7B, interaction modes 1 and 3, respectively). The steric hindrance factor may also participate in PTPα's slowed diffusion, considering that Ag addition leads to 70% immobilization of IgE-FcεRI. These immobilized FcεRI nanoclusters would be expected to obstruct the diffusion of PTPα and other mobile TM proteins. From superresolution imaging, we estimate that Ag-clustered FcεRI (dimension about 80 nm) would occupy about 5% of the membrane surface area (14), which would be an increase over any diffusion obstacles present in the membrane, prior to or created by Ag stimulation. Theoretical studies show that even a small level of immobile objects can significantly slow the diffusion of mobile objects in 2D systems (60, 61). In particular, the model of Singh et al. (62) predicts that an increase in the surface coverage of immobile objects by 5% reduces diffusion of a mobile object by amounts consistent with our measurements: Diffusion of PTPα-EGFP, a PTPα variant without cytosolic protein modules (PTPα-E-TM-EGFP), and a passive TM probe (YFP-GL-GT46) are all slowed by about 10% (Fig. 7A). Hence, it seems likely that immobilization of Ag-clustered FcεRI contributes to both the exclusion and slowed diffusion of PTPα, although other explanations cannot be ruled out. Overall, our ImFCS measurements of modulated diffusion point to the importance of both lipid-based and steric exclusion processes in protecting Ag-crosslinked IgE-FcεRI, phosphorylated by Lyn, from dephosphorylation from a TM phosphatase.

## Conclusion

As depicted by interaction modes in Fig. 7B, a coordinated synergy of lipid- and protein-based interactions explains how Ag-crosslinking of IgE-FcεRI leads to its suprathreshold tyrosine phosphorylation, both by facilitating access by Lyn kinase and

limiting access by a TM phosphatase. Based on many studies in our and other laboratories, we take the view that the resting cell is poised to respond to a specific stimulus and that the change in membrane organization to initiate signaling is subtle (15). The subtlety of the change has made detection challenging, requiring superresolution imaging, SPT, and other technically difficult approaches. The strength of the mechanism proposed in Fig. 7B rests on precise ImFCS measurements of small but distinctive diffusion shifts stimulated by Ag for multiple structural variants of the key signaling components and passive probes. Although this suggested mechanism is based primarily on diffusion measurements, these are both internally consistent and consistent with previous studies cited herein. In particular, we showed directly and provided the strongest evidence to date that Lyn's lipid-based steering is necessary to initiate tyrosine phosphorylation. Overall, we demonstrated the relative ease of applying ImFCS, using multiple probes and conventional fluorophores, to dissect contributions of structural features to weak interactions that collectively have decisive impact in stimulated TM signaling. We expect that ImFCS and the experimental strategies described herein will be widely applicable to advance understanding of TM signaling where plasma membrane organization is likely to play an integral role.

## Materials and Methods

Images for ImFCS, DRM, and immunostaining were collected using a home-built TIRF microscope equipped with an electron multiplying charge coupled device (EMCCD) camera (14). The raw images were further processed using ImageJ/FIJI (73) and Igor Pro (version 8; WaveMetrics) routines to determine diffusion coefficient (*D*) values (ImFCS) and *R* values (DRM). The FRAP experiments were conducted on a Zeiss 710 confocal microscope. Detailed descriptions of instrumental setups, image processing, data fitting, and error analyses are provided in *SI Appendix*. The source of all materials including chemicals and plasmids as well as preparation protocols of fixed and live cell samples are also provided in *SI Appendix*.

**Data Availability.** All study data are included in the article and/or *SI Appendix*.

**ACKNOWLEDGMENTS.** We thank Prof. Jeremy Baskin (Cornell University) for the access of the confocal microscope and Alex Batrouni for helping with the imaging especially during pandemic restrictions. We thank Henry Phan and Boyu Yin for discussions on the DRM preparations. This work is supported by National Institute of General Medical Sciences (NIGMS) Grant R01GM117552. The content is solely the responsibility of the authors and does not necessarily represent the official views of NIGMS or NIH.

1. A. Sigalov, Multi-chain immune recognition receptors: Spatial organization and signal transduction. *Semin. Immunol.* **17**, 51–64 (2005).
2. X. Su et al., Phase separation of signaling molecules promotes T cell receptor signal transduction. *Science* **352**, 595–599 (2016).
3. A. D. Douglass, R. D. Vale, Single-molecule microscopy reveals plasma membrane microdomains created by protein-protein networks that exclude or trap signaling molecules in T cells. *Cell* **121**, 937–950 (2005).
4. N. L. Andrews et al., Actin restricts FcεRI diffusion and facilitates antigen-induced receptor immobilization. *Nat. Cell Biol.* **10**, 955–963 (2008).
5. D. Holowka, B. Baird, Roles for lipid heterogeneity in immunoreceptor signaling. *Biochim. Biophys. Acta* **1861** (8 Pt B), 830–836 (2016).
6. D. Holowka et al., Lipid segregation and IgE receptor signaling: A decade of progress. *Biochim. Biophys. Acta* **1746**, 252–259 (2005).
7. V. Bugajev, M. Bambousková, L. Dráberová, P. Dráber, What precedes the initial tyrosine phosphorylation of the high affinity IgE receptor in antigen-activated mast cell? *FEBS Lett.* **584**, 4949–4955 (2010).
8. J. Goyette, D. J. Nieves, Y. Ma, K. Gaus, How does T cell receptor clustering impact on signal transduction? *J. Cell Sci.* **132**, jcs226423 (2019).
9. S. K. Pierce, Lipid rafts and B-cell activation. *Nat. Rev. Immunol.* **2**, 96–105 (2002).
10. S. Bálint, M. L. Dustin, Localizing order to boost signaling. *eLife* **6**, e25375 (2017).
11. M. D. Resh, Regulation of cellular signalling by fatty acid acylation and prenylation of signal transduction proteins. *Cell. Signal.* **8**, 403–412 (1996).
12. J. Rivera, A. M. Gilfillan, Molecular regulation of mast cell activation. *J. Allergy Clin. Immunol.* **117**, 1214–1225, quiz 1226 (2006).
13. J. Rivera, N. A. Fierro, A. Olivera, R. Suzuki, New insights on mast cell activation via the high affinity receptor for IgE. *Adv. Immunol.* **98**, 85–120 (2008).
14. S. A. Shelby, D. Holowka, B. Baird, S. L. Veatch, Distinct stages of stimulated FcεRI receptor clustering and immobilization are identified through superresolution imaging. *Biophys. J.* **105**, 2343–2354 (2013).
15. S. A. Shelby, S. L. Veatch, D. A. Holowka, B. A. Baird, Functional nanoscale coupling of Lyn kinase with IgE-FcεRI is restricted by the actin cytoskeleton in early antigen-stimulated signaling. *Mol. Biol. Cell* **27**, 3645–3658 (2016).
16. T. Kambayashi, G. A. Koretzky, Proximal signaling events in FcεRI-mediated mast cell activation. *J. Allergy Clin. Immunol.* **119**, 544–552, quiz 553–554 (2007).
17. M. Wu, D. Holowka, H. G. Craighead, B. Baird, Visualization of plasma membrane compartmentalization with patterned lipid bilayers. *Proc. Natl. Acad. Sci. U.S.A.* **101**, 13798–13803 (2004).
18. A. M. Davey, K. M. Krise, E. D. Sheets, A. A. Heikal, Molecular perspective of antigen-mediated mast cell signaling. *J. Biol. Chem.* **283**, 7117–7127 (2008).
19. A. M. Davey, R. P. Walvick, Y. Liu, A. A. Heikal, E. D. Sheets, Membrane order and molecular dynamics associated with IgE receptor cross-linking in mast cells. *Biophys. J.* **92**, 343–355 (2007).
20. E. D. Mitra, S. C. Whitehead, D. Holowka, B. Baird, J. P. Sethna, Computation of a theoretical membrane phase diagram and the role of phase in lipid-raft-mediated protein organization. *J. Phys. Chem. B* **122**, 3500–3513 (2018).
21. E. Sezgin, I. Levental, S. Mayor, C. Eggeling, The mystery of membrane organization: Composition, regulation and roles of lipid rafts. *Nat. Rev. Mol. Cell Biol.* **18**, 361–374 (2017).
22. K. A. Field, D. Holowka, B. Baird, FcεRI-mediated recruitment of p53/56lyn to detergent-resistant membrane domains accompanies cellular signaling. *Proc. Natl. Acad. Sci. U.S.A.* **92**, 9201–9205 (1995).
23. P. S. Pyenta, D. Holowka, B. Baird, Cross-correlation analysis of inner-leaflet-anchored green fluorescent protein co-redistributed with IgE receptors and outer leaflet lipid raft components. *Biophys. J.* **80**, 2120–2132 (2001).
24. R. M. Young, X. Zheng, D. Holowka, B. Baird, Reconstitution of regulated phosphorylation of FcεRI by a lipid raft-excluded protein-tyrosine phosphatase. *J. Biol. Chem.* **280**, 1230–1235 (2005).
25. K. A. Field, D. Holowka, B. Baird, Structural aspects of the association of FcεRI with detergent-resistant membranes. *J. Biol. Chem.* **274**, 1753–1758 (1999).

26. E. D. Sheets, D. Holowka, B. Baird, Critical role for cholesterol in Lyn-mediated tyrosine phosphorylation of FcεpsilonRI and their association with detergent-resistant membranes. *J. Cell Biol.* **145**, 877–887 (1999).
27. F. M. Goñi, "Rafts": A nickname for putative transient nanodomains. *Chem. Phys. Lipids* **218**, 34–39 (2019).
28. P. Sengupta *et al.*, Probing protein heterogeneity in the plasma membrane using PALM and pair correlation analysis. *Nat. Methods* **8**, 969–975 (2011).
29. S. L. Veatch *et al.*, Correlation functions quantify super-resolution images and estimate apparent clustering due to over-counting. *PLoS One* **7**, e31457 (2012).
30. M. Kinoshita *et al.*, Raft-based sphingomyelin interactions revealed by new fluorescent sphingomyelin analogs. *J. Cell Biol.* **216**, 1183–1204 10.1083/jcb.201607086 (2017).
31. I. Koyama-Honda *et al.*, High-speed single-molecule imaging reveals signal transduction by induced transbilayer raft phases. *J. Cell Biol.* **219**, e202006125 (2020).
32. N. Bag, D. A. Holowka, B. A. Baird, Imaging FCS delineates subtle heterogeneity in plasma membranes of resting mast cells. *Mol. Biol. Cell* **31**, 709–723 (2020).
33. B. Kannan *et al.*, Spatially resolved total internal reflection fluorescence correlation microscopy using an electron multiplying charge-coupled device camera. *Anal. Chem.* **79**, 4463–4470 (2007).
34. D. Lingwood, K. Simons, Detergent resistance as a tool in membrane research. *Nat. Protoc.* **2**, 2159–2165 (2007).
35. A. K. Menon, D. Holowka, W. W. Webb, B. Baird, Clustering, mobility, and triggering activity of small oligomers of immunoglobulin E on rat basophilic leukemia cells. *J. Cell Biol.* **102**, 534–540 (1986).
36. P. S. Pyenta, P. Schwillie, W. W. Webb, D. Holowka, B. Baird, Lateral diffusion of membrane lipid-anchored probes before and after aggregation of cell surface IgE-receptors. *J. Phys. Chem. A* **107**, 8310–8318 (2003).
37. A. Pralle, P. Keller, E.-L. Florin, K. Simons, J. K. Hörber, Sphingolipid-cholesterol rafts diffuse as small entities in the plasma membrane of mammalian cells. *J. Cell Biol.* **148**, 997–1008 (2000).
38. A. K. Kenworthy *et al.*, Dynamics of putative raft-associated proteins at the cell surface. *J. Cell Biol.* **165**, 735–746 (2004).
39. P. Sengupta *et al.*, A lipid-based partitioning mechanism for selective incorporation of proteins into membranes of HIV particles. *Nat. Cell Biol.* **21**, 452–461 (2019).
40. H. W. Sohn, P. Tolar, T. Jin, S. K. Pierce, Fluorescence resonance energy transfer in living cells reveals dynamic membrane changes in the initiation of B cell signaling. *Proc. Natl. Acad. Sci. U.S.A.* **103**, 8143–8148 (2006).
41. M. B. Stone, S. A. Shelby, M. F. Núñez, K. Wisser, S. L. Veatch, Protein sorting by lipid phase-like domains supports emergent signaling function in B lymphocyte plasma membranes. *eLife* **6**, e19891 (2017).
42. T. Zech *et al.*, Accumulation of raft lipids in T-cell plasma membrane domains engaged in TCR signalling. *EMBO J.* **28**, 466–476 (2009).
43. M. F. Núñez, K. Wisser, S. L. Veatch, Synergistic factors control kinase-phosphatase organization in B-cells engaged with supported bilayers. *Mol. Biol. Cell* **31**, 667–682 (2020).
44. E. K. Fridriksson *et al.*, Quantitative analysis of phospholipids in functionally important membrane domains from RBL-2H3 mast cells using tandem high-resolution mass spectrometry. *Biochemistry* **38**, 8056–8063 (1999).
45. P. Pathak, E. London, Measurement of lipid nanodomain (raft) formation and size in sphingomyelin/POPC/cholesterol vesicles shows TX-100 and transmembrane helices increase domain size by coalescing preexisting nanodomains but do not induce domain formation. *Biophys. J.* **101**, 2417–2425 (2011).
46. D. Holowka, K. Thanapuaswan, B. Baird, Short chain ceramides disrupt immunoreceptor signaling by inhibiting segregation of Lo from Ld Plasma membrane components. *Biol. Open* **7**, bio034702 (2018).
47. D. R. Larson, J. A. Gosse, D. A. Holowka, B. A. Baird, W. W. Webb, Temporally resolved interactions between antigen-stimulated IgE receptors and Lyn kinase on living cells. *J. Cell Biol.* **171**, 527–536 (2005).
48. N. L. Andrews *et al.*, Small, mobile FcεpsilonRI receptor aggregates are signaling competent. *Immunity* **31**, 469–479 (2009).
49. J. H. Lorent *et al.*, Plasma membranes are asymmetric in lipid unsaturation, packing and protein shape. *Nat. Chem. Biol.* **16**, 644–652 10.1038/s41589-020-0529-6 (2020).
50. P. Sengupta, A. Hammond, D. Holowka, B. Baird, Structural determinants for partitioning of lipids and proteins between coexisting fluid phases in giant plasma membrane vesicles. *Biochim. Biophys. Acta* **1778**, 20–32 (2008).
51. W. Rodgers, Making membranes green: Construction and characterization of GFP-fusion proteins targeted to discrete plasma membrane domains. *Biotechniques* **32**, 1044–1046, 1048, 1050–1051 (2002).
52. T. Baumgart *et al.*, Large-scale fluid/fluid phase separation of proteins and lipids in giant plasma membrane vesicles. *Proc. Natl. Acad. Sci. U.S.A.* **104**, 3165–3170 (2007).
53. E. Ingley, Functions of the Lyn tyrosine kinase in health and disease. *Cell Commun. Signal.* **10**, 21 (2012).
54. S. Hammond, A. Wagenknecht-Wiesner, S. L. Veatch, D. Holowka, B. Baird, Roles for SH2 and SH3 domains in Lyn kinase association with activated FcεpsilonRI in RBL mast cells revealed by patterned surface analysis. *J. Struct. Biol.* **168**, 161–167 (2009).
55. A. J. Torres, L. Vasudevan, D. Holowka, B. A. Baird, Focal adhesion proteins connect IgE receptors to the cytoskeleton as revealed by micropatterned ligand arrays. *Proc. Natl. Acad. Sci. U.S.A.* **105**, 17238–17244 (2008).
56. D. L. Wakefield, D. Holowka, B. Baird, The FcεRI signaling cascade and integrin trafficking converge at patterned ligand surfaces. *Mol. Biol. Cell* **28**, 3383–3396 10.1091/mbc.E17-03-0208 (2017).
57. M. Kovárová *et al.*, Structure-function analysis of Lyn kinase association with lipid rafts and initiation of early signaling events after Fcεpsilon receptor I aggregation. *Mol. Cell Biol.* **21**, 8318–8328 (2001).
58. K. A. Field, D. Holowka, B. Baird, Compartmentalized activation of the high affinity immunoglobulin E receptor within membrane domains. *J. Biol. Chem.* **272**, 4276–4280 (1997).
59. N. Bag, S. Huang, T. Wohland, Plasma membrane organization of epidermal growth factor receptor in resting and ligand-bound states. *Biophys. J.* **109**, 1925–1936 (2015).
60. Z. Kalay, T. K. Fujiwara, A. Otaka, A. Kusumi, Lateral diffusion in a discrete fluid membrane with immobile particles. *Phys. Rev. E Stat. Nonlin. Soft Matter Phys.* **89**, 022724 (2014).
61. N. Oppenheimer, H. Diamant, In-plane dynamics of membranes with immobile inclusions. *Phys. Rev. Lett.* **107**, 258102 (2011).
62. R. R. Singh, A. S. Sangani, S. Daniel, D. L. Koch, The combined hydrodynamic and thermodynamic effects of immobilized proteins on the diffusion of mobile transmembrane proteins. *J. Fluid Mech.* **877**, 648–681 (2019).
63. D. Holowka, B. Baird, Nanodomains in early and later phases of FcεRI signalling. *Essays Biochem.* **57**, 147–163 (2015).
64. A. Honigsmann, A. Pralle, Compartmentalization of the Cell Membrane. *J. Mol. Biol.* **428** (24 Pt A), 4739–4748 (2016).
65. A. K. Kenworthy, Have we become overly reliant on lipid rafts? Talking Point on the involvement of lipid rafts in T-cell activation. *EMBO Rep.* **9**, 531–535 (2008).
66. D. A. Brown, Lipid rafts, detergent-resistant membranes, and raft targeting signals. *Physiology (Bethesda)* **21**, 430–439 (2006).
67. A. G. Lee, Lipid-protein interactions. *Biochem. Soc. Trans.* **39**, 761–766 (2011).
68. B. B. Machta, S. L. Veatch, J. P. Sethna, Critical Casimir forces in cellular membranes. *Phys. Rev. Lett.* **109**, 138101 (2012).
69. H. Turner, J.-P. Kinet, Signalling through the high-affinity IgE receptor FcεRI. *Nature* **402**, B24–B30 (1999).
70. E. Ingley, Src family kinases: Regulation of their activities, levels and identification of new pathways. *Biochim. Biophys. Acta* **1784**, 56–65 (2008).
71. J. D. Mohr, "Characterizing membrane receptor signaling: New roles for electrostatic residues in EGFR regulation and actin in FcεRI signaling," PhD dissertation, Biomedical and Biological Sciences (2019).
72. J. L. Thomas, D. Holowka, B. Baird, W. W. Webb, Large-scale co-aggregation of fluorescent lipid probes with cell surface proteins. *J. Cell Biol.* **125**, 795–802 (1994).
73. J. Schindelin *et al.*, Fiji: An open-source platform for biological-image analysis. *Nat. Methods* **9**, 676–682 (2012).